PROCEEDINGS OF SPIE

SPIEDigitalLibrary.org/conference-proceedings-of-spie

Customized packaged bolometers in niche applications at INO

Bruno Fisette, Francis Généreux, David Béland, Patrice Topart, Mathieu Tremblay, et al.

Bruno Fisette, Francis Généreux, David Béland, Patrice Topart, Mathieu Tremblay, Yan Desroches, Marc Terroux, Linda Marchese, Christian Proulx, Francis Picard, Denis Dufour, Alain Bergeron, François Châteauneuf, Christine Alain, "Customized packaged bolometers in niche applications at INO," Proc. SPIE 10656, Image Sensing Technologies: Materials, Devices, Systems, and Applications V, 106560H (14 May 2018); doi: 10.1117/12.2303513

Event: SPIE Commercial + Scientific Sensing and Imaging, 2018, Orlando, Florida, United States

Customized packaged bolometers in niche applications at INO

Bruno Fisette*, Francis Généreux, David Béland, Patrice Topart, Mathieu Tremblay, Yan Desroches, Marc Terroux, Linda Marchese, Christian Proulx, Francis Picard, Denis Dufour, Alain Bergeron, François Châteauneuf and Christine Alain
INO, 2740 Einstein Street, Quebec, Quebec, Canada, G2P 4S4

ABSTRACT

This paper reviews recent developments in customized packaged bolometers at INO with an emphasis on their applications. The evolution of INOs bolometer packages is also presented. Fully packaged focal plane arrays of broadband microbolometers with expanded absorbing range are shown, for applications in spectroscopic and THz imaging. This paper also reports on the development of customized packaged bolometer focal plane arrays (FPAs) for space applications such as a multispectral imaging radiometer for fire diagnosis, a far infrared radiometer for in-situ measurements of ice clouds and a net flux radiometer for Mars exploration.

Keywords: Infrared, Terahertz Uncooled, Microbolometer, 35 µm, Gold black, Packaging, Focal Plane Array

1. INTRODUCTION

INO has been active in the development of customized uncooled bolometers since the early 1990s[1-6]. INOs microbolometers are used in several fields, including security applications[6-7], Earth observation from space[3-5] and airborne applications such as the far infrared sensing of thin ice clouds[8-10]. As uncooled microbolometers require a pressure below 10 mTorr to work efficiently[11], INO has also been active in vacuum sealed packaging for more than 20 years[2,12-14]. INO has especially been involved in the development of packaging of bolometer FPAs for space applications, such as the New Infrared Sensor Technology (NIRST) instrument, one of the payloads of the SAC-D/Aquarius satellite launched in 2011, for which INO supplied the IR camera module[15].

This paper reviews the recent development of customized packaged bolometers at INO with an emphasis on their applications. The following section briefly describes the evolution of microbolometers and their associated packaging solutions at INO over more than 20 years. Section 3 presents the main characteristics and performances of a fully packaged focal plane array of broadband bolometers and its use as the core of a portable Long Wave InfraRed (LWIR) hyperspectral imager based on a MEMS Fabry-Perot interferometer. The Section 4 presents a fully packaged focal plane array of THz bolometers and an inspection system based on it that detects items such as powders, liquid or electronics inside mail envelopes. In the Section 5, several space applications based on customized packaged bolometers are described.

2. EVOLUTION OF PACKAGED BOLOMETERS AT INO

2.1 Microbolometers

Microbolometer activities at INO started originally with 52µm pitch pixels on 128x128 arrays for use in the 8-12µm wavelength range[16]. They were based on vanadium oxide thin films. INO's next step was to increase the performance and the array size, by moving to 160x120 arrays with 52 µm pitch pixels in the early 2000's[2], as applications in imagery constantly drive the need for ever bigger arrays. In parallel, 256x1 linear arrays for spectroscopic applications were also developed using 52µm pixel technology[2]. In the late 2000's, a new linear array of 512x3 pixels with a pixel pitch of 39µm was developed specifically for space applications[17]. For thermal imaging applications, the quest for ever-increasing image resolution led INO, and the rest of the bolometer industry[18-19], to further reduce the pixel pitch and increase the array size.

*Bruno.Fisette@ino.ca; phone 1 418 657-7006; fax 1 418 657-7009; www.ino.ca

Image Sensing Technologies: Materials, Devices, Systems, and Applications V, edited by
Nibir K. Dhar, Achyut K. Dutta, Proc. of SPIE Vol. 10656, 106560H · © 2018 SPIE
CCC code: 0277-786X/18/$18 · doi: 10.1117/12.2303513

For the last decade, INO has successively developed a 35μm pitch pixel for 384x288 arrays[6], as well as 17μm [20] and 12μm pitch pixels[21]. The following table shows the Noise Equivalent Temperature Difference (NETD), the response time and the Figure of Merit (FOM) in the 8-12μm wavelength band for the most recently developed pixels.

Table 1. Performance summary of INO microbolometers as a function of their pixel pitch (previously reported[21]).

Bolometer pitch (μm)	Pulse rate (Hz)	NETD (mK)	Response time (ms)	FOM (ms*mK)	State-of-the-art (ms*mK)
35	30	14	12.6	177	150[22], 60 Hz
17	60	29.5	8.35	246	240[23], 30 Hz
12	60	72.8	3.87	282	353[24], 30 Hz
12	120	73.3	4.67	342	353[24], 30 Hz

In parallel to the quest for smaller pixels, INO has also worked to develop customized bolometer designs for specific applications. For example, in far infrared radiometry where larger pixels were required, INO's 160x120 FPA with 52μm pixel pitch was adapted to become a 80x60 matrix with 104μm pixel pitch[8]. Another example of pixel customization is bolometer design optimization for use in other wavelength ranges. An example of optimization for the MidWave Infrared (MWIR) region will be presented in section 5.

2.2 Packaging

Packaging is a key element in the miniaturization and cost reduction of microbolometer FPAs[25]. In parallel with the evolution of bolometer FPAs, the technologies required to package them have also evolved. From the original metal flat-pack packages[2], ceramic leaded packages[2] and die-level packages[11], INO has migrated to two main families of packaging solutions.

To address commercial applications requiring low cost, reduced footprint and high throughput production, a TECless ceramic leadless chip carrier (LCC) technology has been developed[26]. This package is presented on figure 1. For this package family, the die cavity can be as small as 16 mm squared with a thickness of 1.4 mm. This package is vacuum sealed during the soldering of the germanium window to the package header inside a vacuum furnace. By using a non-evaporable getter technology and by pumping out the gas load emitted during the window soldering process, the lifetime of the product is extended to more than 10 years.

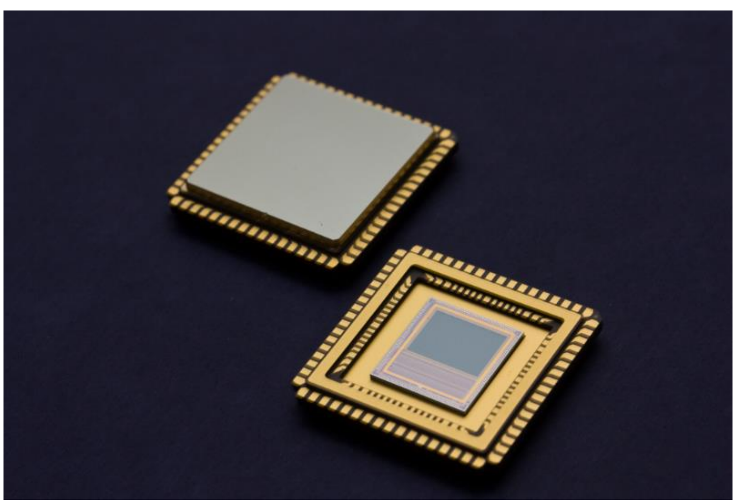

Figure 1. INO's ceramic 68LCCC package equipped with a germanium window

To address high end applications, especially space applications where reliability and customization are the main drivers, a second family of packaging solutions has been developed[14]. This packaging solution is based on a kovar header including high-temperature co-fired ceramic to hermetically seal the electrical feedthroughs. A metallic cover containing the window is hermetically joined to the base and, thereafter, the overall package is heated and pumped out using an oxygen-free copper tube. The tube is then pinched to vacuum-seal the package. Figure 2 presents an example of a package based on this technology. Electrically activated getters are inserted inside the package cavity to extend the lifetime to a target of 25 years.

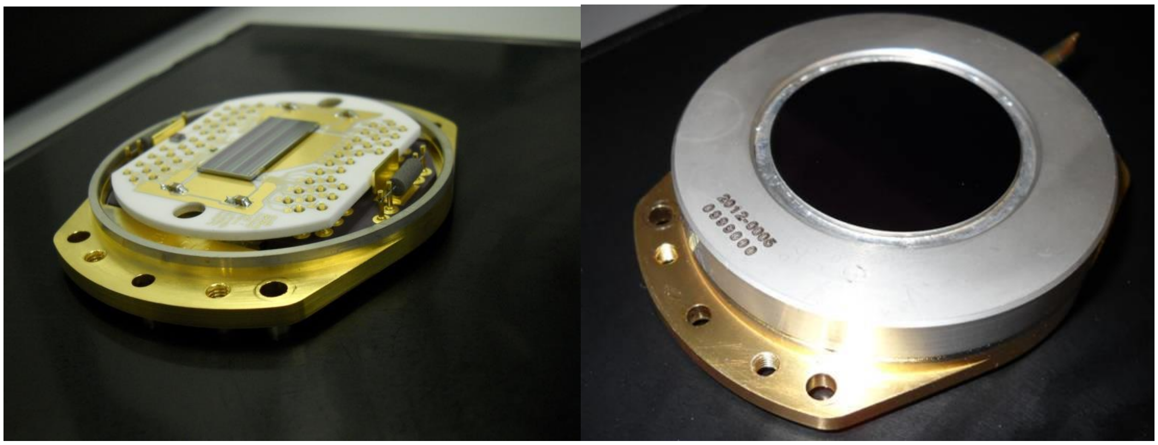

Figure 2. High reliability package base assembly (left) and Vacuum sealed high reliability package (right)

To monitor the pressure inside the package cavity, INO has developed MEMS micropirani gauges based on VOx bolometer microfabrication processes. These pressure gauges have a measurement range from 10^{-3} Torr to 1 atm. Their typical accuracy is ±5% from 3 mTorr to 10 mTorr. Their operation method was described in detail in previous papers[27-28].

3. BROADBAND APPLICATIONS

In this section, customized solutions for broadband applications in the 3-14 μm wavelength range are described. To enhance the spectral absorption of uncooled microbolometer pixel arrays, the FPAs were coated with a 25 µm thick gold black thin film deposited using an evaporation process performed at INO. Spectroscopic measurements obtained for various deposition conditions and film thicknesses showed that the specular reflectance of the gold black coating is less than 10 % in the wavelength range from 0.2 to 100 µm which makes it an excellent broadband absorber for both infrared and terahertz radiation[29]. A graph of the typical gold black specular reflectance percentage as function of wavelength is presented in Figure 3.

The gold black layer inherently creates a thermal short between the bolometer pixels. To singulate and preserve the electrical and thermal isolation of each pixel[29-31], narrow trenches are made in the gold black layer using a laser trimming process developed at INO. To laser-trim an entire 384 x 288 pixel matrix, a high speed laser station with micrometric accuracy was used. Trench widths smaller than 4 µm are produced in gold black layers by using picosecond laser pulses (Δt = 35 ps) at a wavelength of 532 nm with a high beam quality ($M^2 < 1.2$), thus preserving a significant fill factor. The laser pulses are emitted from a fiber laser source in a Master Oscillator – Power Amplification architecture developed at INO (MOPAW) that emits 25 W of IR power at repetition rates ranging from single shot to 1 MHz. The laser includes a sophisticated modulated seed system that generates arbitrarily shaped pulse envelopes with durations varying from 2.5 ns to 500 ns and containing one or multiple ps or ns pulses[32]. Precision motorized XY-Theta stages coupled to a high-resolution vision system allows for the positioning of the microbolometer FPA to an accuracy of better than 1 µm with respect to the focused laser spot.

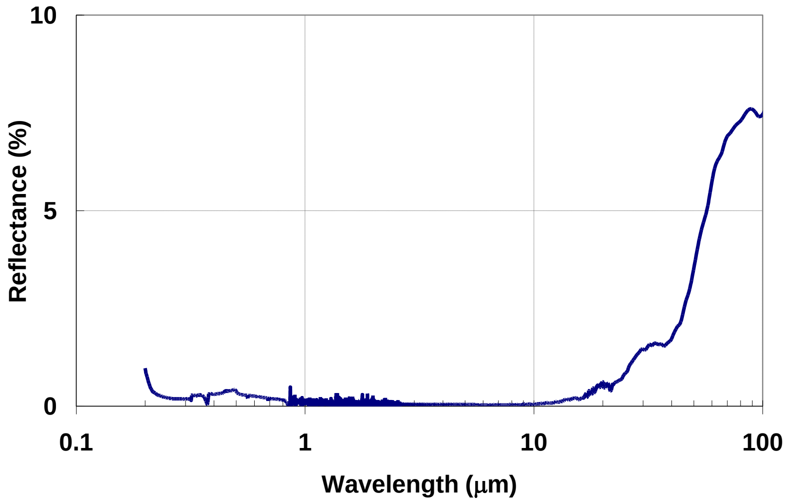

Figure 3. Specular reflectance of a 31 µm gold black film measured between 0.2 µm and 100 µm.

3.1 Vacuum packaged 384x288 broadband bolometer FPA for applications in the 3-14 µm wavelength range

The main challenge in packaging gold-blackened FPAs is the sintering of the gold black layer at high temperature. The packaging process already developed for high reliability applications was adapted to limit the exposure of the gold-blackened FPA to low temperatures[10,33]. Also, the footprint was reduced to 32 x 36 mm^2, the detector to be driven with a smaller electronic interface (MicroXcam)[34]. The cross-section of the MicroXcam electronic core is 57 mm x 57 mm in size, allowing for the development of small imaging systems. Figure 4 presents the vacuum packaged 384x288 broadband bolometer FPA with enhanced absorption in the 3-14 µm wavelength range.

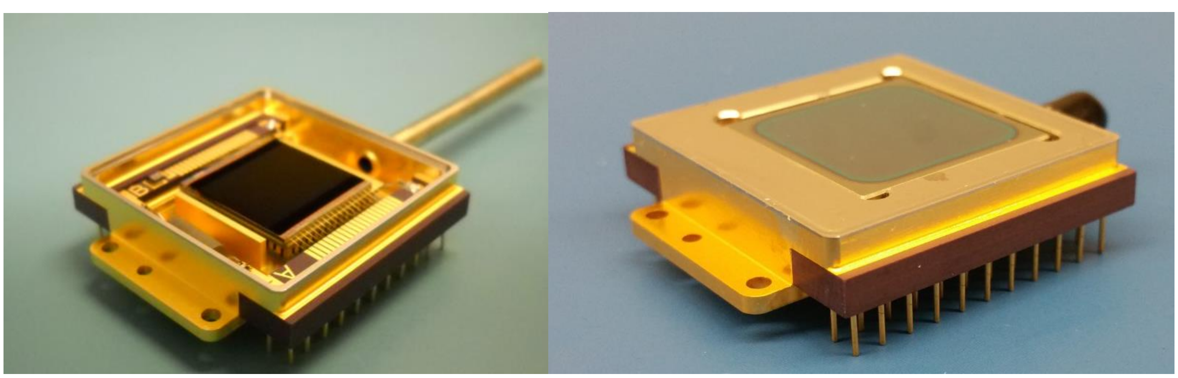

Figure 4. Vacuum-sealed package for broadband applications in the 3-14µm wavelength

The performances of this device are presented in terms of Noise Equivalent Power (NEP) and detectivity. Measurements were performed under dynamic vacuum pumping prior to vacuum sealing of the packages. A dynamic pumping approach was favored to remove the contribution of the package base pressure on the performance. The following tests were performed on two different 384 x 288 bolometer FPAs packaged using the same process. The first FPA is a standard INO 384 x 288 without gold black, and the second is the updated INO 384 x 288 FPA with gold black.

The methodology used to measure the NEP in the packages has been described in a previous paper[14]. In this work, the NEP was characterized for scene temperatures ranging between 20°C and 40°C. The following measurement parameters were used: broadband AR-coated Ge window (3-14 µm wavelength), integration time = 40µs, F-number = F/1, TEC temperature = 25°C and frame rate = 50 Hz. The estimated error on NEP measurement is 5%. The NEP of the standard INO 384 x 288 FPA is 72 pW on the 3-14μm wavelength range. The updated INO 384 x 288 FPA with gold black shows a lower NEP value of 26 pW. Figure 5 illustrates the relative NEP as function of the wavelength. As shown on this plot, the NEP for the updated INO 384 x 288 FPA with gold black is not only lower, it is also more uniform over the entire spectral band thanks to the flat absorption spectrum of the gold black thin film.

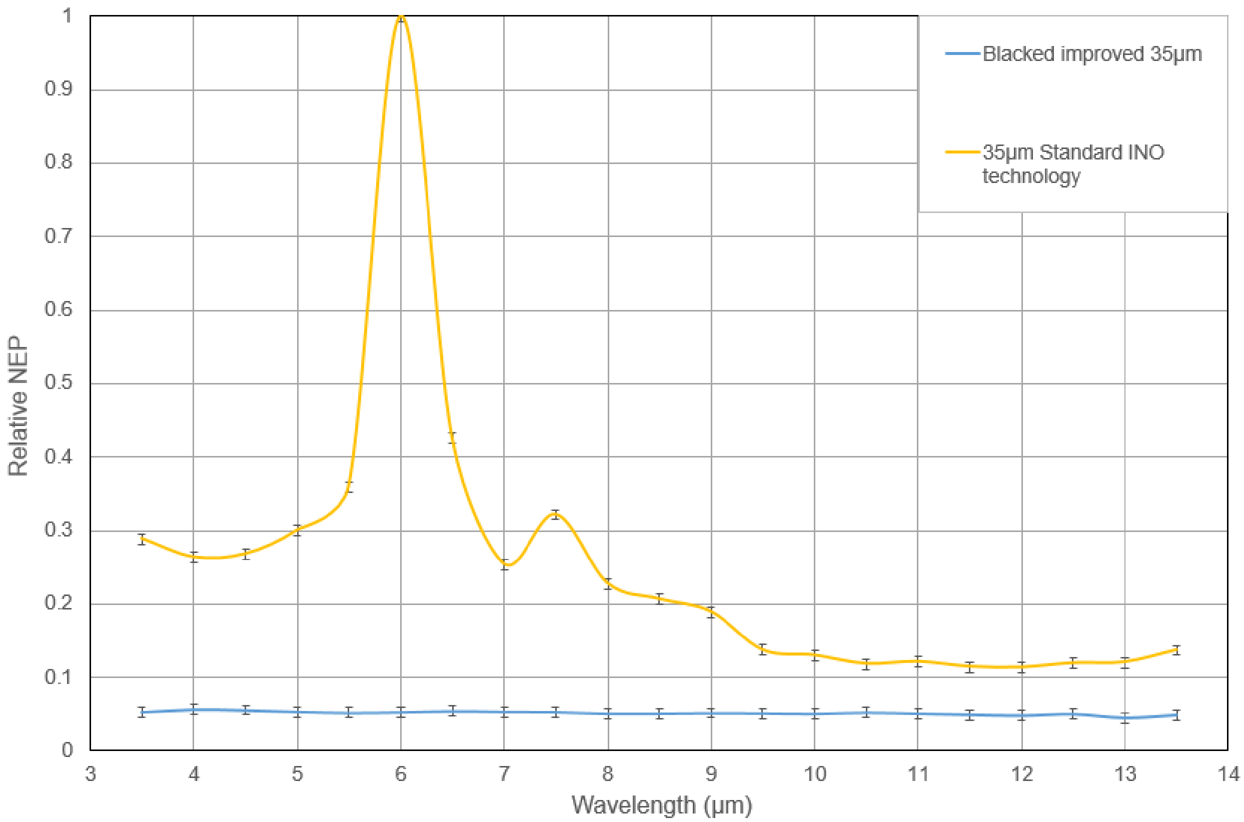

Figure 5. Relative NEP as function of wavelength for INO's standard 384 x 288 FPA and the updated 384 x 288 FPA with gold black.

The methodology used to measure the detectivity in the packages has been described in a previous paper[33]. In this work, the spectral responsivity over the wavelength range from 3-14μm was measured with a monochromator. The spectral resolution of the monochromator exit slit was set to 50 nm. Figure 6 shows the relative detectivity thus obtained. For wavelengths below 8 μm, the detectivity is more than 5 times higher for the new INO 384 x 288 FPA with gold black. Also, as for the NEP, the detectivity is uniform over the whole spectral band.

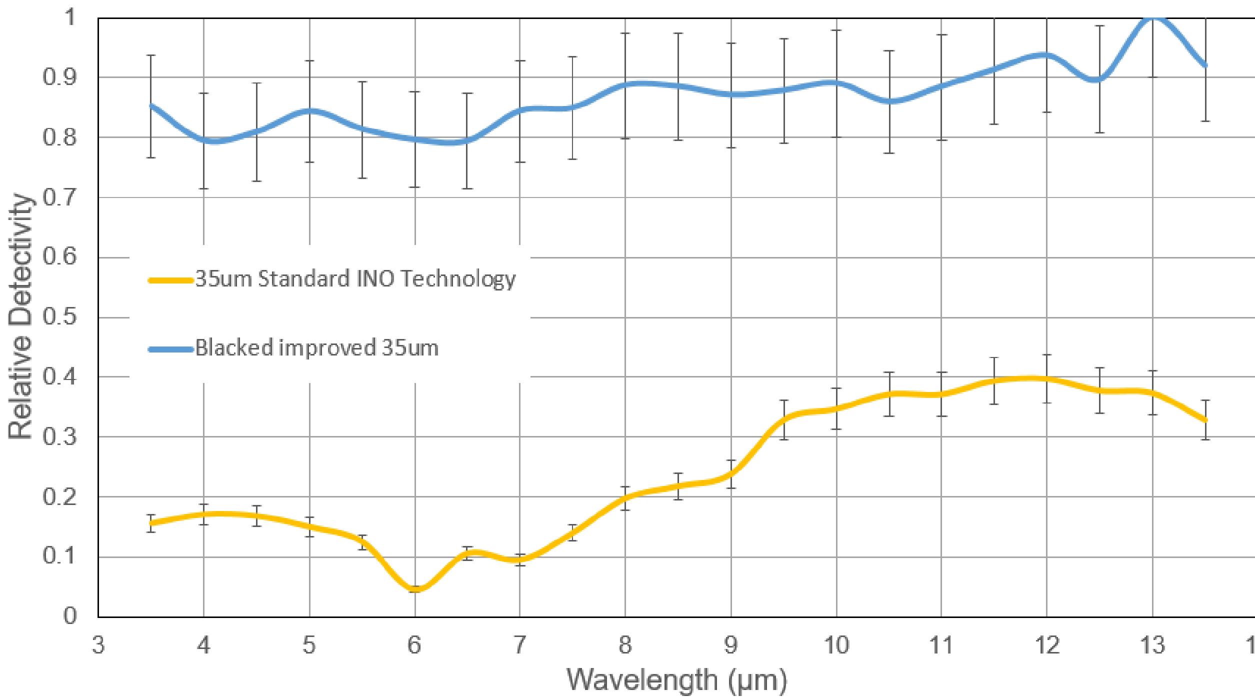

Figure 6. Detectivity of packaged FPAs from 3.5 to 13.5µm.

3.2 Portable LWIR hyperspectral imager

The fast-growing consumer electronics market of connected and wearable devices is driving a wealth of new applications. The personal detection and monitoring of substances affecting our everyday life (food, cosmetics, drugs, etc.) will soon become a reality as a number of pocket spectrometers are being reported. These prototypes operate in the visible and near infrared due to the common availability of detectors. However, enhanced selectivity would be obtained by operating instead in the so-called infrared fingerprint region (3-14 µm band). To this end, a compact, portable, long-wave infrared hyperspectral imager was developed. The updated 384x288 FPA with gold black presented in the previous subsection is a good candidate for this application. However, its package size is too large for implementation in a compact spectrometer. To overcome this difficulty, a low temperature process compatible with our LCC packaging technology was developed. The main constraint is still the sintering of gold black at high temperatures. To evaluate if this packaging solution is viable, gold black samples were heated overnight to a maximum temperature at 170°C. The reflectance of the gold black samples was measured before and after the baking test. After baking, the reflectance remained below 1% for wavelengths below 14µm as presented on Figure 7. These measurements indicate that gold black samples could be packaged using LCC packaging technology with a low temperature process for broadband applications in the 3-14µm wavelength range.

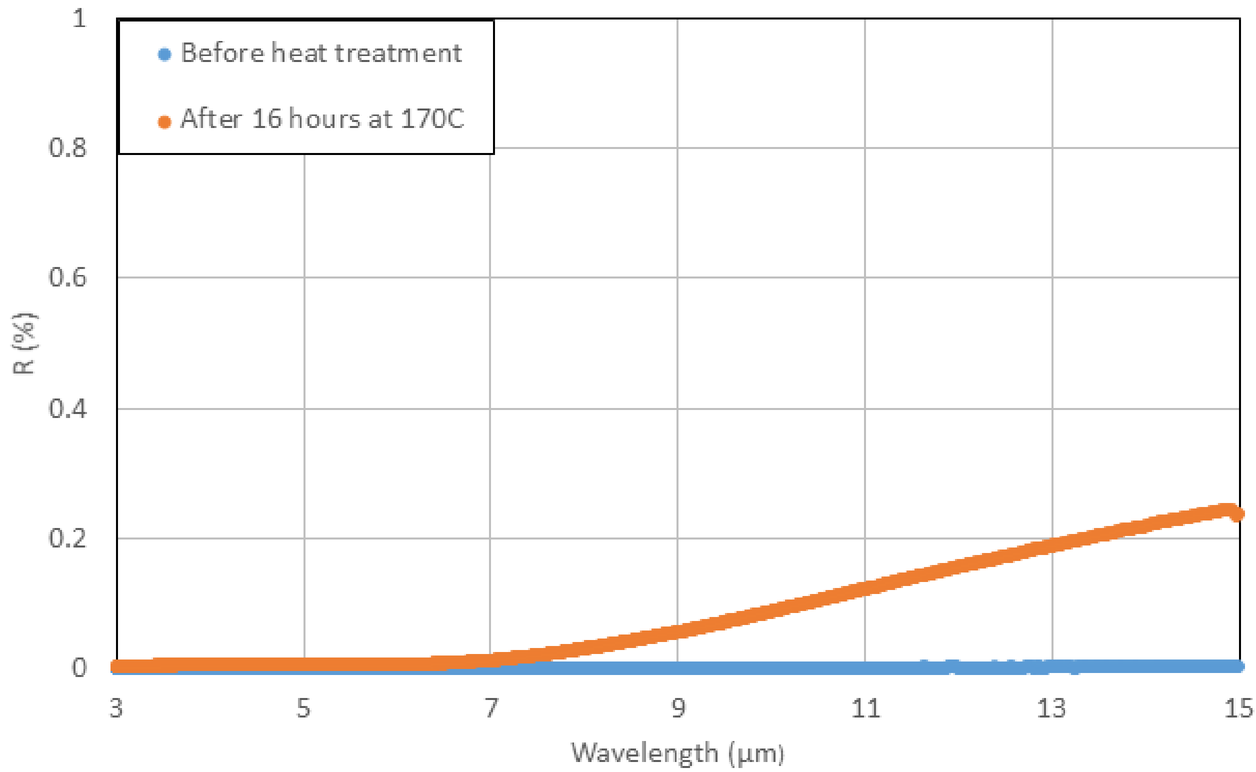

Figure 7. Gold black reflectance before and after 16 hours bakeout with maximum temperature at 170°C.

The LWIR hyperspectral imager is based on this packaged detector, driven by INO's MicroXcam camera and Fraunhofer ENAS' 2 mm x 2 mm MEMS Fabry-Perot Interferometer (FPI)[35]. The size of the hyperspectral imager is approximately 7 cm x 7 cm x 7 cm excluding the source. An example of an IR source currently used for hyperspectral imaging performance tests at INO is the IR-18 model from HawkEye Technologies, providing a power of 18W for an overall size of 2.5mm diameter X 5mm. The source-sample-imaging system can be used either in reflectance mode or in transmission mode. In reflectance mode, the spectral image is the signal acquired with the sample divided by the signal acquired with only a mirror in front of the camera. In transmission mode, the spectral image is the signal acquired with the sample divided by the signal acquired with no sample. The spectral resolution varies from 36 to 200 nm depending on the type of FPI used. The noise equivalent spectral radiance was measured as 660 $mW \cdot sr^{-1} \cdot m^{-2} \cdot \mu m^{-1}$ at 10 µm.

Hyperspectral images of various polymers and substances were recorded in transmittance and reflectance modes. For example, a measured polystyrene transmittance spectrum is presented on Figure 8. A good agreement was found between the measured hyperspectral imager spectrum and the expected spectrum simulated by applying the FPI transfer function to the higher resolution spectrum of the same sample measured with a commercial FTIR. The small difference between the two spectra is likely due to the inaccuracy of the convolution used to extract the transmission data from the commercial FTIR. More details have been presented in another paper[36].

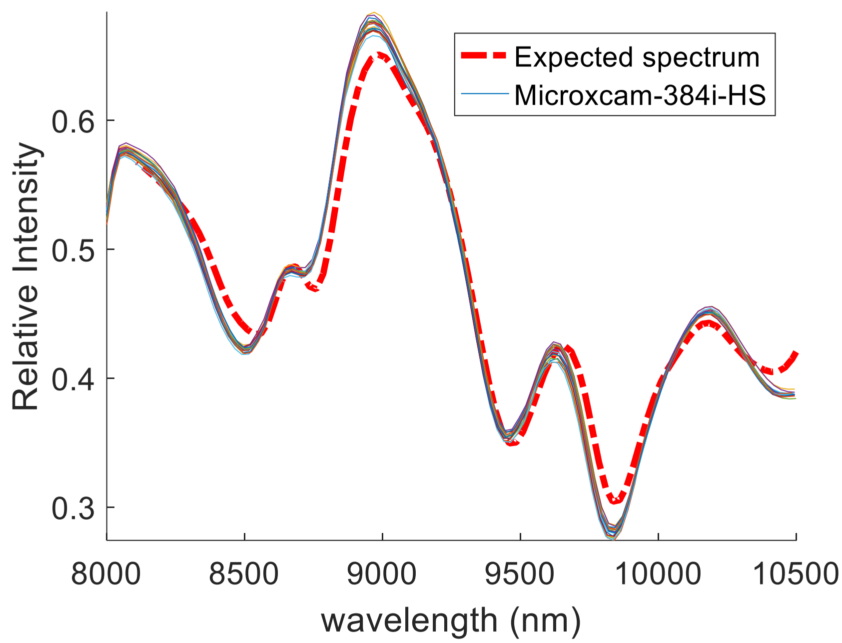

Figure 8. Polystyrene transmittance spectrum measured by the LWIR hyperspectral imager, in comparison with the expected spectrum derived from an FTIR measurement.

4. TERAHERTZ APPLICATIONS

In this section, the vacuum packaged 384x288 broadband bolometer FPA presented in section 3 is slightly modified to extend the high absorbance benefits of gold black to longer wavelengths. Also, an application of this technology in the terahertz wavelength region is described.

4.1 Vacuum packaged 388x288 bolometer FPA for terahertz applications

To increase bolometer responsivity for wavelengths longer than 100 µm, a thicker gold black layer is required to enhance the absorption. For wavelengths higher than 300 µm, laser trimming of the pixels is no longer required, since the 35 µm pixel pitch is far below the diffraction-limited spot size for these illumination wavelengths. Nevertheless, having a pixel pitch below the diffraction limit provides improved image quality in the THz wavelength region due to aliasing and artefact reduction, resulting in an improved overall image sharpness[37].

In addition to the increased gold black layer thickness, another important difference is present in the THz package in comparison with the broadband applications package: the window material is no longer Germanium due to its high absorption for wavelengths longer than 14 µm. High resistivity float zone silicon is instead used for the window due to its extremely wide transmittance range. Indeed, the transmittance is more than 50% in the 1.2µm to 1 mm wavelength range. To minimize the mismatch between the thermal expansion coefficients of the package's cover and its window, the cover material was changed from kovar to invar for the THz version.

Figure 9 shows a typical NEP for the packaged detector designed for the THz wavelength range. The methodology used to measure the NEP in THz packages has been described in a previous paper[38]. The pyroelectric detectors used for this measurement are Gentec TPR-D-69-THz and VDI PM5. The sources used are an Elva BWO and a Coherent SIFIR-50 laser. The following measurement parameters were used: Si-HRFz window, integration time = 40µs, TEC temperature = 24°C and frame rate = 50 Hz. The estimated error of the NEP measurement is less than 10%. The updated INO 384 x 288 FPA with gold black shows a NEP value of 62 pW at a frequency of 282 GHz (i.e. a wavelength of 1063µm). The reported NEPs are lower than the state-of-the-art publicly reported on smaller arrays[39]. Also, as shown in Figure 9, the reported NEP is mostly wavelength independent from the lower wavelengths of the THz region up to 1.5mm than any previously reported results.

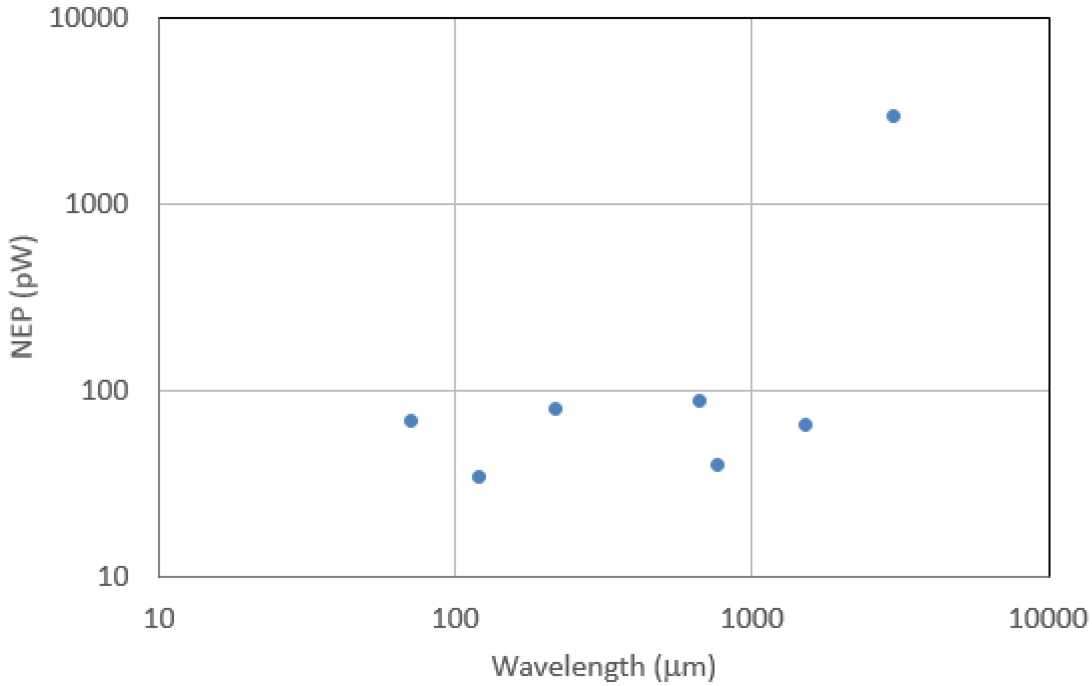

Figure 9. NEP of packaged FPAs from 70 μm to 3000 μm.

These NEPs are obtained with an antireflective parylene coating on the window, optimized for the measured wavelength of interest. The addition of a parylene coating allows to optimize the NEP for a selected wavelength in the range from 60 μm to 3189 μm.

Figure 10 shows an image taken with a reflection imaging setup using a MicroXcam camera with the 384x288 THz packaged detector and a VDI source operating at a frequency of 400GHz with a power of 7mW. This setup allows to see through the plastic exterior of a security access card. In this preliminary test setup, the imaging field of view is restricted to 13mm x 10mm due to the very low output power of the source. A mosaic of scans allows to cover the full 8.5cm x 5.5cm area of the magnetic card. The scans and the mosaicking were performed quickly and no additional image processing has been performed. At this THz frequency, the NEP is as low as 40pW.

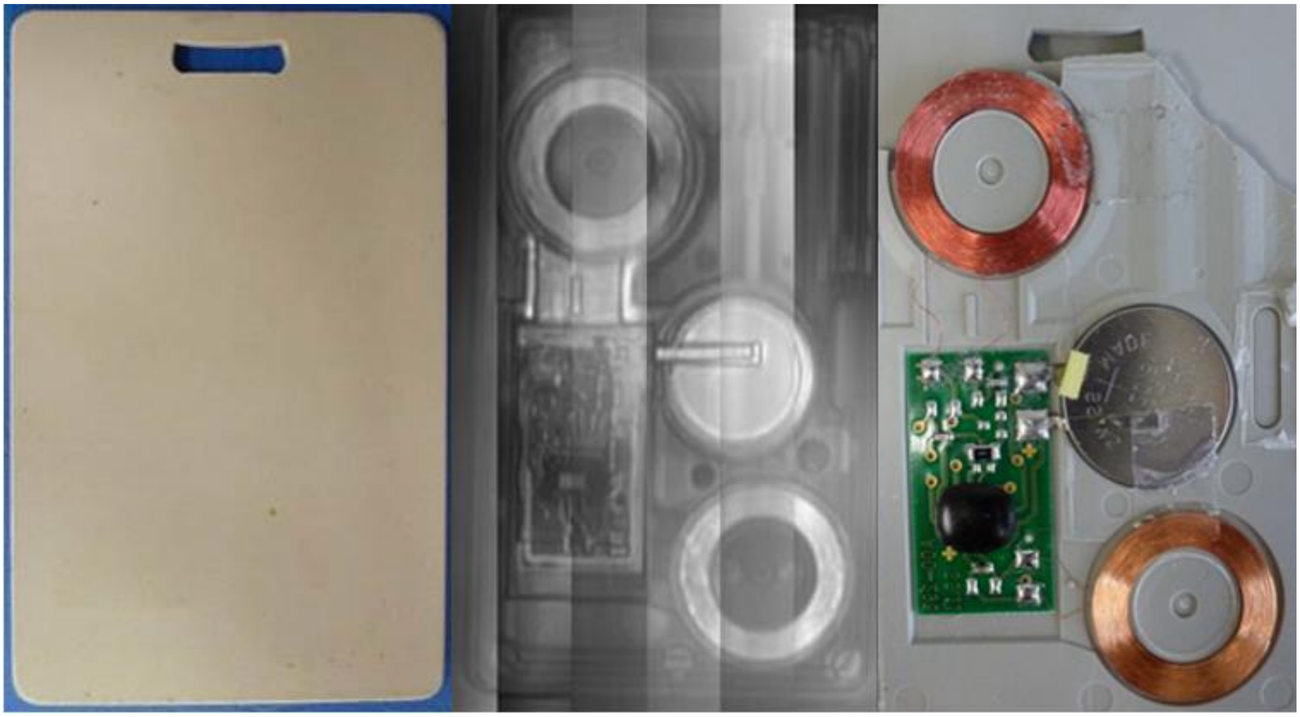

Figure 10. Visible photo of a magnetic card (left), THz image of this card (center) and visible image of a similar card's interior (right)

4.2 Mail inspection system based on terahertz technology

The THz vacuum packaged 384x288 microbolometer FPA previously described is the core of a mail inspection system developed at INO for one of our spinoff companies. This mail inspection system detects items such as powders, liquids or electronics inside mail envelopes. The system was invented to circumvent attacks by mail screening for various organizations, VIPs and mail centers. It is able to see through letters, flat envelopes and small packets. When an operator passes a suspect mail envelope in the viewing area of the system, he sees in real time the THz image of the elements inside the envelope. This technology is safer for the operator with regards to concurrent technologies such as X-Ray. In addition to the INO's terahertz detector, the mail inspection system is equipped with a metal detector.

5. SPACE APPLICATIONS FOR BOLOMETERS

Over the years, INO has developed several packaged bolometer FPAs for various space applications such as the monitoring of fires[13], the thermal tracking of ocean temperature[15] and the measurement of Earth's radiation budget[40]. Generally, space applications require customized detectors to achieve specific performance requirements. In the case of microbolometer-based detectors for space, the required performances can be reached by the appropriate design of the FPA bolometer, the customization of the filters in front of the FPA bolometer and by the heterogeneous assembly of these FPAs. In this section, three recent examples of INO microbolometer detectors developed specifically for space applications are presented.

5.1 Multispectral imaging radiometer for fire diagnosis

Wildfire is a costly and growing issue facing governments, made worse in the context of climate change and the proliferation of wildland-urban interface communities[41-43]. The ability to assess wildfire severity can provide important information in support of firefighting resource management. One way of acquiring this information is to remotely sense the radiance emitted in the mid-wave infrared (MWIR) spectral band by the fire being characterized[44]. This important application has led INO, in collaboration with the Canadian Space Agency, to develop a 512x3 pixel focal plane arrays (FPA) incorporating microbolometers (see Figure 11) specifically designed for this task[45]. In order to enhance the response of these infrared microsensors in the MWIR spectral range, a Salisbury screen[46] was integrated to their structure. Critical parameters of the Salisbury screen including the gap size between the bolometer platform and the substrate and the sheet resistance of a metallic absorber have been adjusted to maximize the absorption and responsivity of these bolometers in the 3.4 to 4.2 µm range. As a result of theoretical analyses and experimental validations, the platform-substrate gap size was fixed to 2.3 µm while the deposition parameters used for the metallic absorber were set to obtain a sheet resistance close to 377 ohms per square.

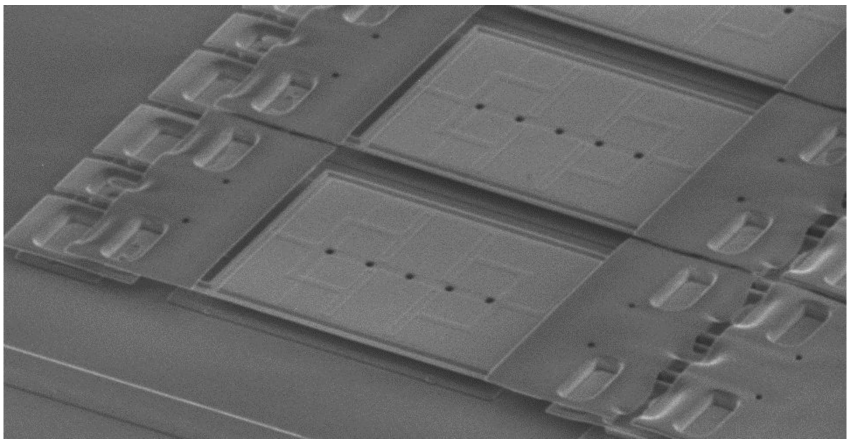

Figure 11. Scanning electron microscope picture of bolometers designed for the 3.4 to 4.2 µm spectral band.

The fabricated bolometers were tested in a so-called half-bridge operation mode, illustrated in Figure 12. For this operation mode, a voltage V is applied to the bolometer under test in series with a test resistor. In this configuration, the bolometer response is maximized by increasing the voltage V until the bolometer resistance R_b becomes equal to the resistance of the test resistor due to Joule heating. For the tests reported here, a test resistor with a resistance of 150 kΩ was used to remove the Joule heating contribution to the thermal conductance

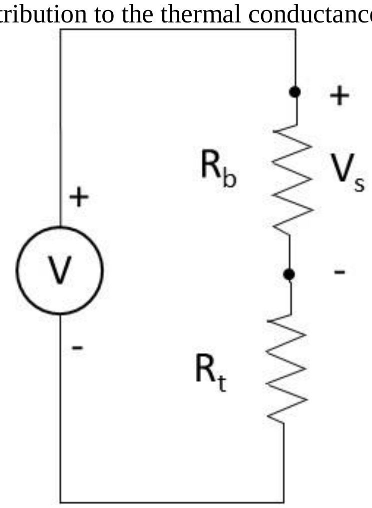

Figure 12. Half-bridge bias circuit used for measuring the bolometer characteristics. R_b is the resistance of the bolometer under test and R_t is the resistance of a test resistor (150 kΩ in this case).

Characteristics of the fabricated bolometers are listed in Table 2 below. As can be seen, these bolometers exhibit the high Thermal Coefficient of Resistance (TCR) typical of bolometric IR sensors based on vanadium oxide. Integrating a Salisbury screen to the bolometer structure enhanced their absorption to a typical value of 86 % for the 3.4 to 4.2 µm wavelength range. It should be noted that the bolometer responsivity is affected by the various constraints dictated by a specific application. In particular, the required response time has an impact on the achievable responsivity. For the specific case reported here, it was important to maintain a response time around 10 ms since this characteristic is directly linked to the achievable ground resolution in a spaceborne remote sensing context. For other applications, a different trade-off can be achieved between response time and responsivity. Longer response times typically allow for an increase of the available responsivity. The typical characteristics of the bolometers developed by INO for a specific wildfire sensing opportunity are shown in Table 2 below.

Table 2. Typical characteristics of bolometers designed for MWIR applications

Parameter	**Typical (std dev)**
Voltage applied to the half-bridge (V)	1.66
Responsivity for the 3.4 to 4.2 µm IR band (V/W)	102 000 (9 000)
Response time (ms)	11.4 (0.3)
Thermal mass (pJ/K)	610 (40)
Effective thermal conductance (nW/K)	53.8 (3.8)
Absorption for the 3.4 to 4.2 µm IR band (%)	86.4 (3.3)
Temperature coefficient of resistance (TCR) for the bolometer vanadium oxide resistor at 22 °C (%/°C)	-2.78

This optimized microbolometer array must be integrated in a package allowing for dynamic vacuum pumping if it is intended to be used in an airborne mission or for terrestrial tests. The wide swath of observation, essential for achieving high revisit rates, is made possible by staggering two 512x3 arrays to form an effective 1017x3 microbolometer array in the detector assembly. This package contains a TEC for thermal control, a routing circuit for electrical interfacing of the arrays, and bandpass filters. The two main challenges for the detector assembly design are: (1) to ensure the high thermal stability environment necessary for accurate radiometric measurements, and (2) to meet the tight alignment requirements between the two staggered arrays, necessary to reach a high degree of parallelism. Analyses of the temperature gradient across the arrays and the thermal radiative environment seen by the pixels were performed in view of achieving the required thermal stability for the arrays. The results obtained allowed us to establish the following design rules: (i) the inner surfaces of the assembly need to be reflective to reduce the effects of thermal emission fluctuations on the arrays; (ii) the substrate of the routing circuit should be thick and have a large thermal conductance to improve the stability of the array; (iii) a low thermal conductance of the epoxy used in the bonding of the arrays and a large cooling area of the TEC are necessary to reduce the thermal gradient across the array; (iv) the filters should be controlled thermally so as to limit their thermal emission fluctuation contribution to the array and (v) a reflective mask should be added to the optical window to minimize the impacts of thermal fluctuations of the optics in front of the detector assembly.

Figure 13 shows the details of the resulting detector assembly. It is composed of a header and a cover, each individually assembled and sealed to each other with bolts and an o-ring. Both parts are made of Kovar and plated with Ni-Au, to ensure a high infrared reflectance. The routing circuit substrate is made of high conductivity AlN (1.7×10^5 W/K) and has the maximum commercially available thickness (1.3 mm) for this material. Following the detector array alignment positioning, the arrays are bonded to the substrate with a low conductivity epoxy. High-precision temperature control of the arrays is provided by a TEC, custom designed to have a cooling area (44x28 mm^2) large enough to be in full thermal contact with both arrays from the back side of the substrate. Not shown in the photographed assembly are two bandpass filters of identical characteristics that are suspended above the arrays. The thermally conductive mechanical supports for each filter are directly mounted on the routing circuit substrate so that the filter is also controlled thermally by the TEC. The cover of the detector assembly is seen to incorporate a reflective mask that minimizes the contribution of thermal radiation outside the field-of-view of the arrays. The recessed position of the mask allows to receive a 2.7-mm thick ZnSe optical window. The size and mass of the completed assembly are respectively 7.6 x 9 x 2.5 cm^3 and 0.35 kg.

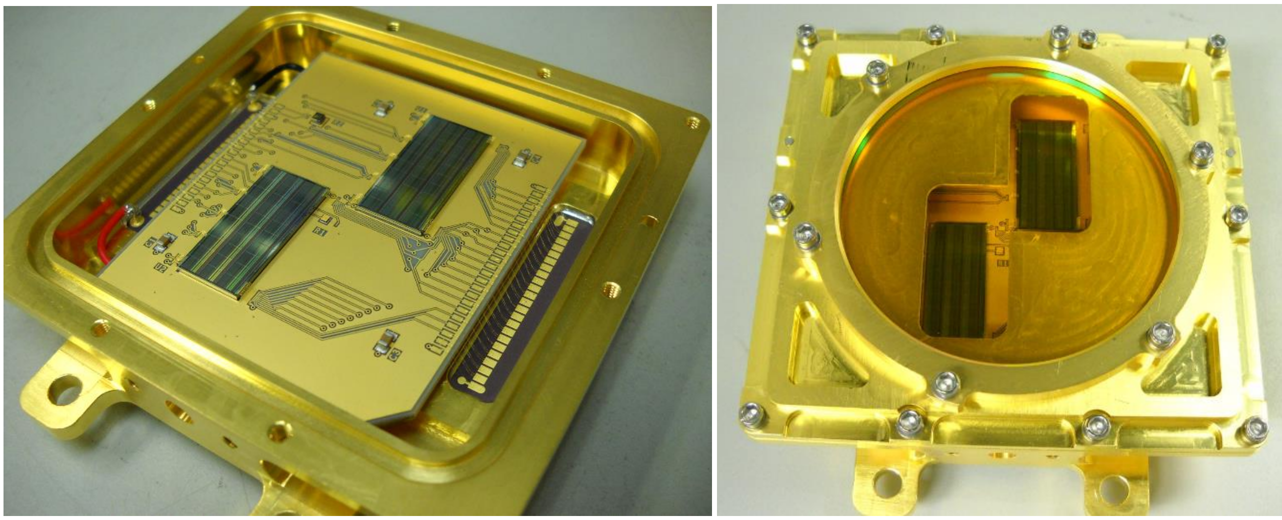

Figure 13. Detector assembly without cover (left) and with cover (right)

The multispectral imaging radiometer for which this detector package was developed is designed to allow for a high co-registration accuracy between the detector pixels of two detectors assemblies: one operating in the MWIR wavelength region and one operating in the LWIR region. The bandpass filters for the MWIR detector cover a wavelength range from 3.4 to 4.2 μm. The LWIR bandpass filter presents a high transmission from 10.4 to 12.3μm. To achieve the co-registration requirement, the detector assemblies for the two cameras are mounted on a common baseplate with a high degree of flatness. During the instrument assembly process, the position of each detector assembly is determined with respect to each other by registering the positions of four alignment features printed on the routing circuit substrate. Using a modified wafer probing station, it is possible to determine the positions of these features to an accuracy of ± 2 μm so as to evaluate the clocking angles with which to rotate the assemblies to optimize their parallelism.

The above methodology assumes that the two individual arrays inside each detector assembly are suitable co-aligned with each other. This alignment is carried out in a similar fashion, using four alignment features deposited on the array and a series of reference features printed onto the routing circuit substrate. The separation between features on the array and routing circuit was measured on high precision translation stages of a microscope. The choice of epoxy used for bonding the detector arrays to the routing circuit is crucial, to minimize movements of the array with respect to the routing circuits during curing. Two detector packages were assembled to validate the chosen package assembly and alignment procedures, as well as the selected epoxy blend. By measuring the positions of the edge pixels of the center lines of the arrays after curing, a positioning error smaller than ±2 μm with respect to a perfectly parallel alignment was observed for both detector packages, as shown in Figure 14.

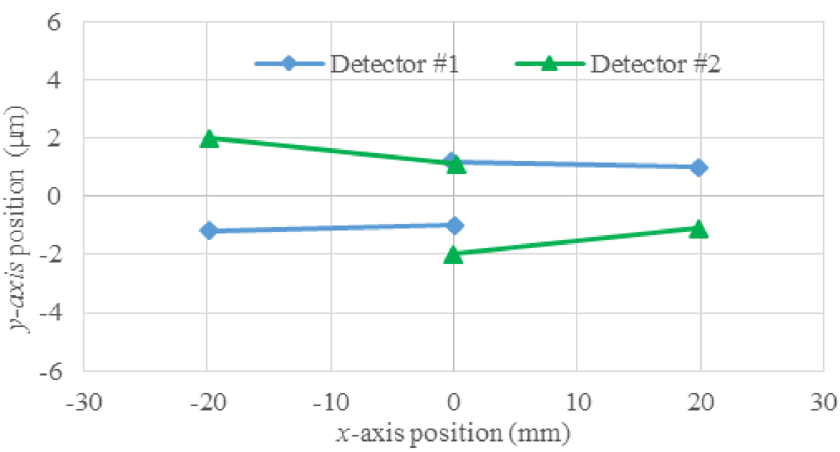

Figure 14. Rotation-corrected and stagger-corrected positions of the edge pixels of the center row for two manufactured detector assemblies

5.2 Far infrared radiometer for in-situ measurements of ice clouds

The far infrared radiometer (FIRR) is an aircraft-certified instrument intended for in-situ measurements of clouds on a modified Basler BT-67 aircraft operated by the Alfred Wegener Institute[8-10]. FIRR was designed to meet the requirements of a pan-arctic airborne mission while meeting the operating conditions of the above aircraft. It was used in a four-week campaign in April 2015 to measure ice cloud characteristics in support of a CSA microsatellite payload study. Figure 15 shows the FIRR instrument.

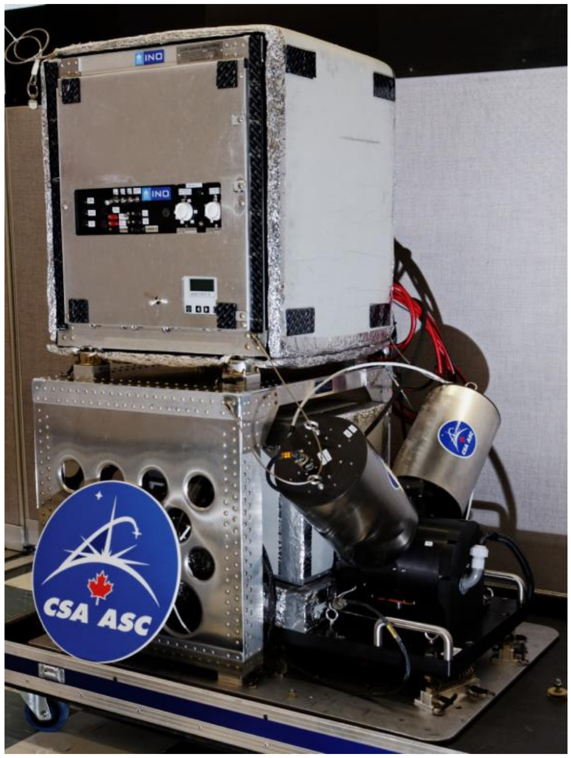

Figure 15. The FIRR instrument ready for the airborne mission.

The core of the instrument is a focal plane array of 80x60 microbolometers that was specially designed with a pitch of 104 µm for far infrared sensing[8]. The focal plane array is monolithically built on a 160x120 CMOS readout integrated circuit (ROIC) with a pitch of 52 µm. The microbolometer structure is designed to receive a gold black coating to enhance the responsivity for wavelengths from 7.9 to 50µm and above. As a result of the narrow field of view selected for the optics in front of the vacuum sealed focal plane array, only a partial area of approximately 316 pixels of the array is illuminated by the scene. Because the camera is intended for non-imaging measurements, this part of the array operates as a single element detector: individual pixel output signals in the illuminated area can be spatially averaged to improve signal-to-noise ratios.

The package selected for this microbolometer is based on the high reliability packaging technology presented in section 2. Customization of the cover assembly was required to reach good transmission in the far infrared wavelength range and to preserve the hermeticity of the package despite the low temperatures encountered during the pan-artic airborne mission. The cover assembly consists of a lid made of invar with nickel plating and a vacuum pumping copper tube. A diamond window is hermetically soldered to the lid to complete the cover assembly. The choice of diamond as an optical window is motivated by the fact that its transmittance (~0.7) is adequate and varies negligibly over the entire targeted spectral range. To develop the diamond window sealing process, finite element analyses and low temperature testing on mock-up packages were performed to identify a suitable solder material and window dimensions. Thermal cycles of 233-293 K were further applied to a comparable package to evaluate the effect of extreme temperatures on the shear stress in the selected window solder. Thermal cycling data suggested that the hermeticity of the detector package is able to withstand the lowest and highest temperatures expected during the airborne mission. As for the other vacuum-sealed packages containing gold blackened FPAs, low temperature processes are required, especially for the vacuum bakeout of the package before sealing. Tests performed throughout the instrument development confirmed that the detector gold black coating was not affected in a detrimental way by the packaging processes. It was verified also that a pressure below 7 mTorr could be maintained effectively in the detector package for a period of at least 18 months under laboratory and flight conditions.

The vacuum-sealed detector is controlled by the INO IRXCAM[47] commercial camera electronics unit, which was made compatible with the developed detector package by the addition of custom electronic and mechanical interfaces. The IRXCAM unit generates readout timings, allows for random access of pixels, supplies bias voltages to the microbolometers, provides for the 16-bit analog-to-digital conversion of the output signal, and transfers data packets to the host computer via an Ethernet connection. Another function of the IRXCAM is to control the feedback loop of the thermoelectric cooler and thermistor so as to maintain the detector operating temperature around a set value.

5.3 Net flux radiometer for Mars exploration

Net flux sensors have been widely used to determine the Earth's surface radiation budget in meteorological applications. They make use of four separate detectors to measure simultaneously the following components of the net radiation: (i) global solar radiation; (ii) ground reflected solar radiation; (iii) sky emitted infrared radiation; and (iv) ground emitted infrared radiation. A net flux radiometer prototype was recently developed by INO to demonstrate the ability of using microbolometers for such an application in the context of Mars exploration. Commercial net flux sensors are usually based on the use of thermopile detectors, in comparison to which microbolometers provide an improved time constant and responsivity. The typical time constant and responsivity of microbolometers used in the prototype are respectively 13 milliseconds and 75 kV/W. Such improvements in performance are the result of the thermal isolation of the bolometer element, achieved in part its immersion in a vacuum environment. The vacuum environment brings additional benefits in that it precludes some issues encountered in thermal detectors. Indeed, it effectively minimizes the convection and conduction of heat to the detector element as well as the sensitivity to external pressure. It also prevents water vapour condensation inside the detector package.

In this work[48], we selected gold-blackened microbolometer detectors of 100-µm size to act as net flux radiometer detectors. Details on the structure of this microbolometer were reported elsewhere[49]. The microbolometer is directly thermally connected to a TEC located in the package base assembly. The TEC is soldered to the package base (which acts as a heat sink) and provides for temperature control of the microbolometer detector. Temperature feedback to the controller is provided by a transistor diode which measures the substrate temperature. A MEMS micropirani gauge is added inside the package cavity to monitor the internal pressure. In addition, an electrically re-fireable getter is integrated into the assembly. The getter has a thermal radiation shield that helps reduce the radiative exchange between the microbolometer and the getter once the latter is activated. The package lid assembly consists of a structural cover and an optical dome providing a detector field of view of 180°. The transmittance of the dome lens also defines the spectral range of sensors. The pyranometer sensor incorporates a fused quartz dome lens with an antireflective coating, providing full transmission in the range from 0.2 µm to 4.5 µm. For the pyrgeometer, a float zone silicon dome coated with an interference filter is used, which provides for a transmission band from 4.5 µm to 50 µm and beyond. Figure 16 shows a photograph of the pyranometer sensor. For this prototype the sensors are used in dynamic vacuum mode.

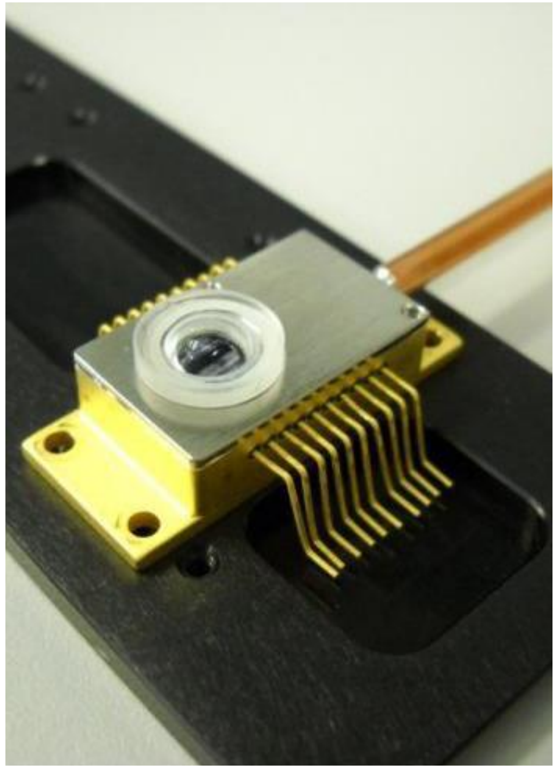

Figure 16. Pyranometer sensor package

6. CONCLUSIONS

In parallel to the development of ever smaller pixels and larger FPA arrays for the thermal imaging, INO has developed several different types of microbolometer detector packages over the past two decades. This paper reviewed some recent developments of customized bolometers at INO with an emphasis on their applications.

A fully packaged focal plane array of broadband microbolometers was presented. This detector makes use of a gold black thin film to expand its absorbing range from 3-14 µm. Thanks to a low temperature packaging process developed to minimize sintering of the gold black absorber during vacuum sealing of the bolometer array package, it shows an NETD lower than 25 mK at a frame rate of 50 Hz. This detector is the core of a portable LWIR hyperspectral imager based on a MEMS Fabry-Perot interferometer.

Another packaged focal plane array adapted for enhanced absorption in the terahertz wavelengths is also described. This detector shows an NEP below 100 pW for wavelengths up to 1.5mm. It can be optimized for different wavelengths of operation in the 60 to 3189µm range. This detector was used to develop an inspection system that detects items such as powders, liquids or electronics inside mail envelopes and small packets.

INO has been involved in the development of customized packaged bolometer FPAs for space applications. The staggered assembly of two 512x3 pixel bolometer FPAs in a package designed for a multispectral imaging radiometer designed for fire diagnosis was shown. This system is based on a bolometer whose absorbance was optimized for applications in the range of 3.4 to 4.2 µm. A far infrared radiometer for in-situ measurements of ice clouds based on customized gold-blackened 104µm pitch pixels was also reported, as was a net flux radiometer for Mars exploration using a sensor package with a field of view of 180°.

ACKNOWLEDGEMENTS

The development of the space applications presented in this paper have been funded by the Canadian Space Agency.
A portion of the work presented in this paper has been funded by the European Space Agency (ESA Contract 400105063/12/NL/NA).

REFERENCES

[1] Jerominek, H., Pope, T.D., Alain, C., Picard, F., Fuchs, R.W., Lehoux, M., Zhang, R., Grenier, C., Rouleau, Y., Cayer, F., Savard, S., Bilodeau, G., Couillard, J.-F. and Larouche, C., "128x128 pixel uncooled bolometric FPA for IR detection and imaging," Proc. SPIE 3436, 585-592 (1998).

[2] Pope, T., Jerominek, H., Alain, C., Cayer, F., Tremblay, B., Grenier, C., Topart, P., LeClair, S., Picard, F., Larouche, C., Boulanger, B., Martel, A. and Desroches, Y. "Commercial and custom 160x120, 256x1, and 512x3 pixel bolometric FPAs " Proc. SPIE 4721, 64-74 (2002).

[3] Pope, T. D., Jerominek, H., Alain, C., Picard, F., Fuchs, R. W., Lehoux, M., Zhang, R., Grenier, C., Rouleau, Y., Cayer, F., Savard, S., Bilodeau, G., Couillard, J.-F. and Larouche, C., "256x1 and 256x40 pixel bolometer arrays for space and industrial applications," Proc. SPIE 3436, 325-331 (1998).

[4] Ngo Phong, L. and Pope, T. D., "Linear arrays of microbolometers for space applications," Proc. 7th IEEE Sensors Conf., 1344-1347 (2008).

[5] Proulx, C., Williamson, F., Allard, M., Baldenberger, G., Gay, D., Garcia-Blanco, S., Côté, P., Martin, L., Larouche, C., Ilias, S., Pope, T., Caldwell, M., Ward, K. and Delderfield, J., "The EarthCARE broadband radiometer detectors," Proc. SPIE 7453, 74530S1-74530S11 (2009).

[6] Chevalier, C., Mercier, L., Duchesne, F., Gagnon, L., Tremblay, B., Terroux, M., Généreux, F., Paultre, J.-E., Provençal, F., Desroches, Y., Marchese, L., Jerominek, H. Alain, C. and Bergeron, A., "Introducing a 384x288 Pixel Terahertz Camera Core," Proc. SPIE 8624, 8624F1-8624F8 (2013).

[7] Marchese, L., Terroux, M., Généreux, F., Tremblay, B., Bolduc, M. and Bergeron, A., "Review of the characteristics of 384x288 pixel THz camera for see-through imaging" Proc. SPIE 8900, 890009-1-890007-7 (2013).

[8] Ngo Phong, L., Proulx, C., Oulachgar, H. and Châteauneuf, F. "Far infrared microbolometers for radiometric measurements of ice cloud" Proc. SPIE 9375, 93750G1-93750G11 (2015).

[9] Libois, Q., Proulx, C., Ivanescu, L., Coursol, L., Pelletier, L.S., Bouzid, Y., Barbero, F., Girard, E. and Blanchet, J.P. "A microbolometer-based far infrared radiometer to study thin ice clouds in the Artic" Atmos. Meas. Tech. 9, 1817-1832 (2016).

[10] Proulx, C., Ngo Phong, L., Lamontagne, F., Wang, M., Fisette, B., Martin, L. and Châteauneuf, F. "Design and instrumentation of an airborne far infrared radiometer for *in-situ* measurements of ice clouds" Proc. SPIE 9973, 99730F (2016).

[11] Garcia-Blanco, Topart, P., Desroches, Y., Caron, J.S., Williamson, F., Alain, C., Pope, T. and Jerominek, H. "Low-temperature vacuum hermetic wafer-level package for uncooled microbolometer FPAs" Proc. SPIE 6884, 68840P1-68840P8 (2008).

[12] Garcia-Blanco, S., Ilias, S., Williamson, F., Généreux, F., Le Noc, L., Poirier, M., Proulx, C., Tremblay, B., Provençal, F., Desroches, Y., Caron, J.S., Larouche, C., Beaupré, P., Fortin, B., Topart, P., Picard, F., Alain, C., Pope, T. and Jerominek, H. "MEMS/MOEMS foundry services at INO" Proc. SPIE 7750, 77500R1-77500R10 (2010).

[13] Topart, P., Picard, F., Ilias, S., Alain, C., Chevalier, C., Fisette, B., Paultre, J.E., Généreux, F., Legros, M., Lepage, J.F., Laverdière, C., Ngo Phong, L, Caron, J.S. and Desroches, Y. "Heteregeneous MEMS device assembly and integration" Proc. SPIE 8975, 89750E1-89750E13 (2014).

[14] Fisette, B., Chevalier, C., Lépine, A., Boucher, M.-A., Larouche, C., Tremblay, M., Lemieux, D., Tremblay, L.-P., Dufour, D., Desroches, Y., Topart, P. and Châteauneuf, F., "Design and fabrication of a scalable high-reliability vacuum sealed package for infrared detectors", 2012 4th Electronic System-Integration Technology Conference 6542149 (2012).

[15] Garcia-Blanco, S., Cote, P., Leclerc, M., Blanchard, N., Desroches, Y., Caron, J.S., Ngo Phong, L., Chateauneuf, F. and Pope, T. "Radiometric packaging of uncooled microbolometer FPA arrays for space applications" Proc. SPIE 7206, 720604-1-720604-12 (2009).

[16] Jerominek, H., Pope, T., Alain, C., Zhang, R., Lehoux, M., Picard, F., Fuchs, W., Grenier, C., Rouleau, Y., Cayer, F., Savard, S., Bilodeau, G., Couillard, J.F., Larouche, C. and Ngo Phong, L., "128 x 128 pixel uncooled bolometric FPA for IR detection and imaging" Proc. SPIE 3436, 585-592 (1998).

[17] Pope, T., Dupont, F., Garcia-Blanco, S., Williamson, F., Chevalier, C., Marchese, L., Chateauneuf, F., Jerominek, H., Ngo Phong, L. and Bouchard, R. "Space qualification of a 512x3 pixel uncooled microbolometer FPA" Proc. SPIE 7298, 729826-1-729826-9 (2009).
[18] Rogalski, A., Martyniuk, P. and Kopytko, M., "Challenges of small-pixel infrared detectors : a review" Reports on Progress in Physics, 79, 046501 (2016).
[19] Skidmore, G.D., Han, C.J. and Li, C., "Uncooled Microbolometers at DRS and Elsewhere Through 2013" Proc. SPIE 9100, 910003-1-910003-5 (2014).
[20] Genereux, F., Provençal, F., Tremblay, B., Boucher, M.-A., Julien, C., and Alain, C., "Vanadium Oxide Thin Film with Improved Sheet Resistance Uniformity" Proc. SPIE 9070, 90701R (2014).
[21] Généreux, F., Tremblay, B., Girard, M., Paultre, J.-E., Provençal, F., Desroches, Y., Oulachgar, H., Ilias, S. and Alain, C., "On the figure of merit of uncooled bolometers fabricated at INO" Proc. SPIE 9819, 98191U1-98191U9 (2016).
[22] Rabaud, W., Vilain M., Meilhan, J., Garret, T., Hopkinson, G., Bentley, M. S., Kraft, S., Legras, O. and Castelein, P., "Uncooled detector development for space application," Proc. SPIE 6958, 69580P1-69580P9 (2008).
[23] Mizrahi, U., Argaman, N., Elkind, S., Giladi, A., Hirsh, Y., Labilov, M., Pivnik, I., Shiloah, N., Singer, M., Tuito, A., Ben-Ezra, M. and Shtrichman, I., "Large format 17µm high-end VOx µ-Bolometer infrared detector," Proc. SPIE 8704, 87041H1-87041H8 (2013).
[24] Becker, S., Imperinetti, P., Yon, J.J., Ouvrier-Buffet, J.L., Goudon, V., Hamelin, A., Vialle, C. and Arnaud, A., "Latest pixel size reduction of uncooled IR-FPA at CEA-LETI," Proc. SPIE 8541, 85410C1-85410C7 (2012).
[25] Cole, B.E, Higashi, R.E., Ridley, J.A. and Wood, R.A., "Integrated vacuum packaging for low-cost light weight uncooled microbolometer arrays" Proc. SPIE 4369, 235 (2001).
[26] Paquet, A., Deshaies, S., Desroches, Y., Whalin, J. and Topart, P., "Influence of the ceramic package internal components on the performance of vacuum sealed uncooled bolometric detectors" Proc. SPIE 8614, 86140G-1-86140G-11 (2013).
[27] Sisto, M.M., Garcia-Blanco, S., Le Noc, L., Tremblay, B., Desroches, Y., Caron, J.S., Provencal, F. and Picard, F., "Pressure sensing in vacuum hermetic micropackaging for MOEMS-MEMS" J. Micro/Nanolith. MEMS MOEMS, 9(4) 041109 (2010).
[28] Sisto, M.M., Garcia-Blanco, S., Le Noc, L., Tremblay, B., Desroches, Y., Caron, J.S., Provencal, F. and Picard, F., "Pressure sensing in vacuum hermetic micropackaging for MOEMS-MEMS" Proc. SPIE 7592, 759204-1-759204-10 (2010).
[29] Ilias, S., Topart, P., Larouche, C., Beaupré, P., Gay, D., Proulx, C., Pope T. and Alain, C. "Deposition and characterization of gold black coatings for thermal infrared detectors" Proc. SPIE 7750, 77501J1-77501J10 (2010).
[30] Becker, W., Fettig, R., Gaymann, A. and Ruppel, W., "Black gold deposits as absorbers for far infrared radiation", Phys. Stat. Sol. (B), 194, pp. 241-255 (1996).
[31] Nelms, N., Dowson, J., Rizvi, N. and Rohr, T., "Laser micromachining of goldblack coatings" Applied Optics, 45(27), 6977-6981 (2006).
[32] Desbiens, L., Deladurantaye, P., Cournoyer, A., Gay, D., Paré, C., Eiselen, S., Roy, V. and Taillon, Y., "Flexible and Programmable Pulse Shaping MOPA Fiber Laser Platform, Performances and Applications, Rev. Laser Eng., Vol 41, No 9, (2013).
[33] Fisette, B., Tremblay, M., Oulachgar, H., Généreux, F., Béland, D., Beaupré, P., Julien, C., Gay, D., Deshaies, S., Terroux, M., Tremblay, B., Dufour, D. and Alain, C., "Novel vacuum packaged 384x288 broadband bolometer FPA with enhanced absorption in 3-14 µm wavelength range" Proc. SPIE 10177, 10177R-1-10177R-15 (2017).
[34] Mercier, L., Fisette, B., Terroux, M., Desroches, Y., Beaupré, P., Demers, M., Dufour, D., Généreux, F., Marchese, L., Topart, P., Alain, C. and Bergeron, A., " Wideband sensitive THz core for application integration" Proc. IRMMW-THz 2015 - 40th Conference on Infrared, Millimeter and Terahertz waves, 7327591 (2015).
[35] Ebermann, M., Neumann, N., Hiller, K., Gittler, E., Meinig, M. and Kurth, S. "Recent advances in expanding the spectral range of MEMS Fabry-Perot filters" Proc. SPIE 7594, 75940V (2010).
[36] Béland, D., Spisser, H., Dufour, D., Le Noc, L, Picard, F. and Topart, P., "Portable LWIR hyperspectral imager based on MEMS Fabry-Perot interferometer and broadband microbolometric detector array", SPIE, To be published
[37] Bergeron, A., Marchese, L., Savard, E., LeNoc, L., Bolduc, M., Terroux, M., Dufour, D., Tang, D., Châteauneuf, F. and Jerominek, H., "Resolution capability comparison of infrared and terahertz imagers" Proc. SPIE 8188, 81880I-1-81880I-8 (2011).

[38] Bolduc, M., Terroux, M., Tremblay, B., Marchese, L., Savard, E., Doucet, M., Oulachgar, H., Alain, C., Jerominek, H. and Bergeron, A., "Noise-Equivalent power characterization of an uncooled microbolometer-base THz imaging camera" Proc. SPIE 8023, 8023-11 (2011).
[39] Rogalski, A. "New Trends in Infrared and Terahertz detectors" 2014 Conference on Optoelectronic and Microlectronic Materials & Devices (COMMAD), 218-220 (2014).
[40] Allard, M., Martin, L., Proulx, C., Bouchard, J.P., Cote, P., Oulachgar, H., Delderfield, J., Parker, D. and Chateauneuf, F. "Current Satus of the EarthCARE BBR Detectors Development" Proc. SPIE 8176, 81761E1-81761E10 (2011).
[41] Wang, X et al. "Increasing frequency of extreme fire weather in Canada with climate change" Climatic Change, 130, 573-586 (2015).
[42] Flannigan, M. et al. "Fuel moisture sensitivity to temperature and precipitation : Climate change implications" Climatic Change, 134, 59-71 (2016).
[43] Massada, A., Radoloff, V., Stewart, S. and Hawbaker, T. "Wildfire risk in the wildland-urban interface : A simulation study in the northwestern Wisconsin" Forest Ecology and Management, 258, 1990-1999 (2009).
[44] Lentille, L, et al. "Remote sensing techniques to assess active fire and post-fire effects" Int. J. Wildland Fire, 15, 319-345 (2006).
[45] Ngo Phong, L., Picard, F., Paultre, J.E., Généreux, F., Dufour, D. and Châteauneuf, F., "Uncooled midwave infrared sensors for spaceborne assessment of fire characteristics" Proc. SPIE 10116, 101160N-1-101160N-11 (2017).
[46] B. A. Munk, Frequency Selective Surfaces: Theory and Design, John Wiley & Sons, Mar. 11, 2005, p. 315.
[47] Le Noc, L., Dufour, D., Terroux, M., Tremblay, B., Lambert, J., Mercier, L., Morrissette, M., Vachon, C., Tang, D. and Bergeron, A. "Towards a very high-resolution infrared camera core" Proc. SPIE 8012, 80123P (2011).
[48] Proulx, C., Ngo Phong, L. and Châteauneuf, F. "Design and fabrication of net flux radiometers for Mars exploration" Proc. SPIE 8975, 897504 (2014).
[49] Ngo Phong, L., Alazzam, A., Daly, M., Proulx, C. and Chateauneuf, F. "Net flux sensor for the measurement of Mars surface radiation budget" Proc. SPIE 8252, 82520A1-82520A12 (2012).